Optical find of hypersonic surface acoustic waves in bulk transparent materials

Rafael J. Jiménez Riobóo,* Alberto Sánchez-Sánchez, and Carlos Prieto
Instituto de Ciencia de Materiales de Madrid (CSIC), c/Sor Juana Inés de la Cruz 3, E-28049-Madrid, Spain
(Received 11 February 2016; revised manuscript received 25 May 2016; published 29 July 2016)

It is shown that direct information from surface acoustic waves (SAWs) of bulk transparent materials can be obtained by using Brillouin light scattering (BLS). The study of surface phonons by means of an optical spectroscopy such as BLS has been historically constrained to nontransparent and highly reflecting bulk and film samples or even to very thin films deposited on reflecting substrates. Probably due to its low signal and to the narrow window in experimental conditions, it was assumed for years that bulk transparent samples were not suited for Brillouin spectroscopy in order to get information on SAWs, negating this optical technique in the search for SAW properties. The reported experiments on transparent glasses and single crystals (cubic MgO and trigonal sapphire) prove that there is no intrinsic physical reason not to collect SAW propagation velocity data from transparent bulk samples and opens a challenge to apply the Brillouin spectroscopy in a wider scenario to obtain direct information, in a nondestructive and contactless way, about SAWs in bulk materials.

DOI: 10.1103/PhysRevB.94.014313

I. INTRODUCTION

The study of surface acoustic waves (SAWs) has been crucial in the understanding of elastomechanical properties of thin films in the fields of hard coatings and electromechanical couplings in the case of sensors and frequency filters in mobile technology [1,2]. Information about SAW propagation velocities can be obtained by standard interdigital transducer (IDT) techniques and network analysis but also by means of optical spectroscopy. The first implies the deposition of metallic structures on the sample surface, thus modifying the sample permanently. On the other hand, optical spectroscopy provides a nondestructive and contactless method to obtain such information. This optical spectroscopy is known as surface Brillouin light scattering (SBLS). Unfortunately since the statement of Sandercock [3]: 'it has so far proved impossible to observe the Rayleigh mode in any transparent material. Opacity is evidently a requirement.' it has been assumed that only nontransparent surfaces could provide this information. In fact, in order to obtain SAW information from transparent films or samples it was usual to cover the transparent surface with a thin metallic coating (between 20 and 40 nm thick) in order to enhance the coupling factor between photons and surface ripples [4]. However, this thin metallic coating modifies the SAW response of the system and only by combining experimental data with numerical simulation techniques was it possible to obtain the desired information about the transparent material [5–8]. In the case of thin transparent samples on reflecting substrates, the SAW propagation velocity of the coating has been successfully gained [9–12] but it was interpreted as an effect of the reflecting properties of the substrate. As expected, in all these cases backscattering geometry was the unique choice. More recently, there have been reports on SAW modes obtained by SBLS in transparent polymeric films on transparent substrates using an unconventional scattering setup for SBLS that allows transmission measurements [13]. The question arises whether SBLS is also able to provide surface information from transparent bulk samples without any modification in their surface. There is some evidence that this can be possible, for instance in a Chemical Vapor Deposition-diamond bulk sample [14]. In this case a SAW mode (Rayleigh mode) together with the shear and the longitudinal bulk modes was detected and evaluated. The aim of this work is to prove that detection of SAW modes on transparent bulk samples is possible for SBLS, opening an additional path for SAW studies. For this purpose, a microscope cover glass, a standard microscope slab, and single-crystalline MgO and sapphire substrates were studied.

II. EXPERIMENT

As indicated above, the samples studied were a standard microscope slab from Labbox (standard line, 1 mm thick), a circular cover glass also from Labbox (standard line, about 150 μm thick), a single-crystalline MgO substrate (500 μm thick), and a single-crystalline sapphire substrate (500 μm thick) with both sides polished from Mateck GmbH. In all cases the samples were transparent and the surfaces were of very high optical quality.

Their optical properties can be summarized in Fig. 1, where the angular and polarization-direction dependences of the reflectivity are shown. The SBLS experimental setup is made up of a 2060 Beamlok Spectra Physics Ar-ion single-mode laser, $\lambda = 514.5$ nm, as monochromatic light source, and a tandem (3 + 3)-pass Fabry-Pérot interferometer [15] as Brillouin spectrometer. Depending on the acoustic modes investigated (bulk or surface), the incoming light will be polarized either in the scattering plane (p polarized) or perpendicular to it (s polarized). p polarization allows coupling between photons and SAW modes.

The well-known 90A scattering geometry [16] [Fig. 2(a)] has been used to obtain the v_L and v_T values at room temperature of the different samples. From the values of v_L and v_T it is possible to obtain a theoretical value for the SAW propagation velocity v_{SAW}. Following Farnell, in the case of

*rjimenez@icmm.csic.es

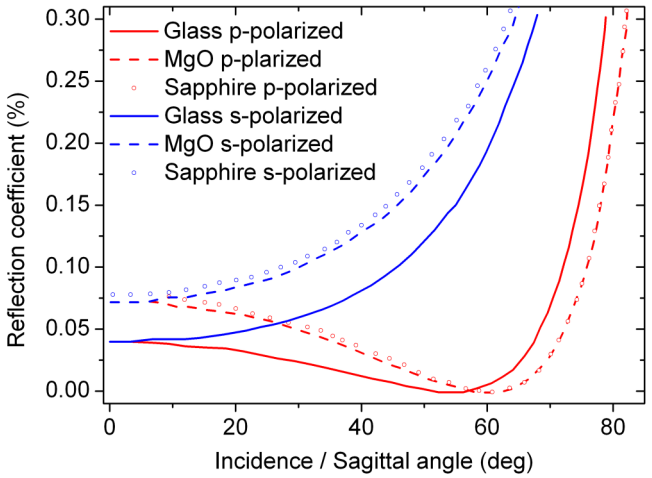

FIG. 1. Dependence of the reflection coefficient on the incident angle and the polarization direction; *p*-polarized (red) and *s*-polarized (blue) for room temperature and $n_{514.5} = 1.5$ [glass (full line)], $n_{514.5} = 1.7439$ [MgO (dashed line)], and $n_{514.5} = 1.7648$ [sapphire (open circles)] obtained by solving Fresnel's equations (more information throughout the text).

an elastically isotropic material (as is the case of the glass samples), the value of v_{SAW} can be obtained by solving the following equation [17]:

$$4\sqrt{\left(1-\frac{v_{\mathrm{SAW}}^2}{v_T^2}\right)\left(1-\frac{v_{\mathrm{SAW}}^2}{v_L^2}\right)}-\left[2-\left(\frac{v_{\mathrm{SAW}}}{v_T}\right)^2\right]^2=0. \tag{1}$$

Some simplifications have been proposed to this equation (see, for instance, Refs. [17,18]):

$$v_{\mathrm{SAW}} = v_T\,\frac{2.87\,v_L^2-4v_T^2}{3\,v_L^2-4v_T^2};$$
$$v_{\mathrm{SAW}} = v_T\,\frac{2.865\,v_L^2-4.004\,v_T^2}{3\,v_L^2-4v_T^2}. \tag{2}$$

The numerical solution of Eq. (1) is the way to obtain the v_{SAW} value from the v_T and v_L values for glass samples. Since this procedure cannot be applied in the case of crystalline samples, in these cases the v_{SAW} values will be obtained from numerical simulation methods [19].

Backscattering geometry will be used to couple to surface acoustic modes in the different samples with the hope of obtaining the corresponding experimental value of v_{SAW}. The sample-air interface, especially in films, can induce a supplementary scattering geometry ($2\alpha A$) [20]. The principle of this scattering geometry is depicted in Fig. 2(b).

III. RESULTS AND DISCUSSION

In the first place, high-resolution Brillouin spectroscopy (HRBS) with standard *s*-polarized incident light and no analysis of the scattered light was performed on the glass samples. In the case of the 90A scattering geometry, the acoustic wave vector lies within the sample and is parallel to the faces of the sample [see Fig. 2(a)], having an absolute value of $q^{90A} = 4\pi\sin(\pi/4)/\lambda_0$ and the corresponding sound velocity of $v_{L,T} = 2f^{L,T}\lambda_0/\sin(\pi/4)$, where the indices L and T represent the longitudinal and shear modes, respectively, and f is the Brillouin frequency shift.

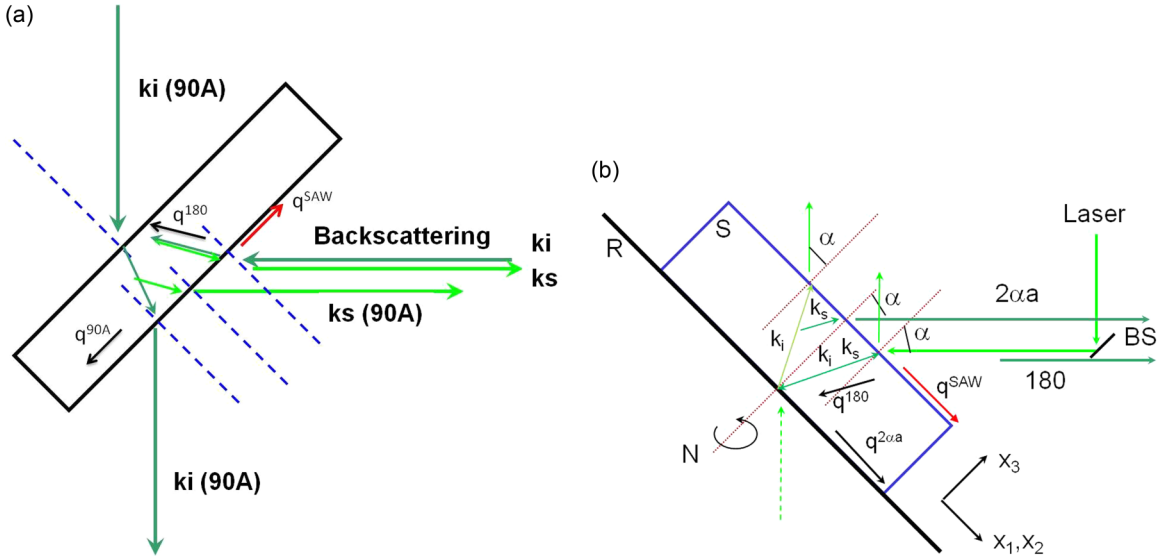

FIG. 2. (a) Schematics of the 90A and backscattering (180) geometries. k_i and k_s are the corresponding incident and scattered light wave vectors. The different acoustic wave vectors (q) are indicated in their corresponding directions. In the case of backscattering geometry the possible surface acoustic wave vector is shown as a red arrow. (b) Schematics of the 2αA and backscattering (180) geometries. S is the sample and R is the reflecting substrate (in our case R is simply the glass-air interface). α is the incident angle or scattering angle or sagittal angle. k_i and k_s are the corresponding incident and scattered light wave vectors. The different acoustic wave vectors (q) are indicated in their corresponding directions. In the case of backscattering geometry the possible surface acoustic wave vector is shown as a red arrow.

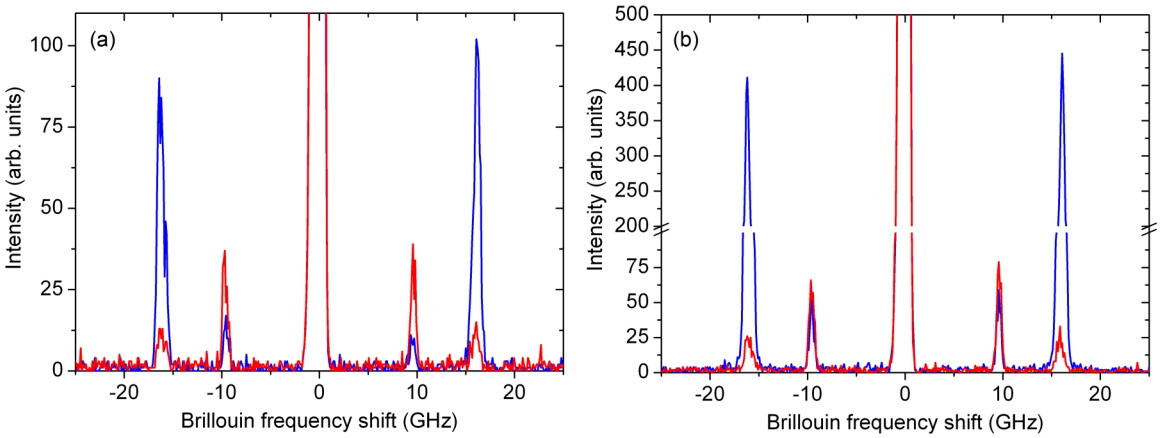

FIG. 3. HRBS spectra of (a) the microscope slab in 90A scattering geometry and (b) the cover glass in 90A scattering geometry for two different polarizations of the incident light, *s* polarized (blue) and *p* polarized (red).

In order to couple the incident photons with the thermal surface acoustic modes it is necessary that the incident light is polarized within the scattering plane (*p* polarization). Figure 3 shows the difference in the spectra obtained in the 90A scattering geometry with *s* and *p* polarization for both glass samples. There is an interchange in intensity between the Brillouin peaks related to the shear mode and those to the longitudinal mode.

Now let us focus our attention on the air-glass interface in backscattering geometry. In order to assure that the scattering information is being gathered as near to the surface as possible, the incident beam is focused on the sample surface and not within the volume, as is usual in backscattering geometry. In this scattering configuration the size of the scattering volume (about 100 μm in diameter) is similar to the sample thickness in the case of the cover glass sample, and the back glass surface can act as a reflecting substrate, thus introducing a new scattering geometry (the 2αA) that plays an important role. If the same experiment as above is performed in this configuration with a sagittal angle (scattering angle) $\alpha = 65^\circ$ one obtains very interesting cover glass Brillouin spectra like the one shown in Fig. 4(b). The same scenario can be observed in the case of the thicker (1 mm) glass slab [Fig. 4(a)].

The standard backscattering contribution is located at about 30 GHz and lies outside the area shown; with the *s* polarization one observes Brillouin peaks corresponding to the *T* and *L* acoustic modes in 130A scattering geometry, as expected, but in the *p* polarization only Brillouin peaks corresponding to the *T* acoustic mode and to an acoustic mode of lower frequency can be seen. The Brillouin peak associated with the *L* acoustic mode has vanished. It is also important to notice that, with the *p* polarization, the reflectivity of the sample surface diminishes dramatically due to the fact that the scattering angles are not very far from the Brewster angle of glass (about 56°, Fig. 1). It has been stated that surface reflectivity is crucial in order to obtain Brillouin peaks related to the SAW modes but *p* polarization is the one that couples photons to SAW modes. In transparent samples *p* polarization implies almost no reflection on the sample surface, and thus the odds of observing a SAW mode should be very limited, almost zero. However, the BS spectrum does show an extra low-frequency mode.

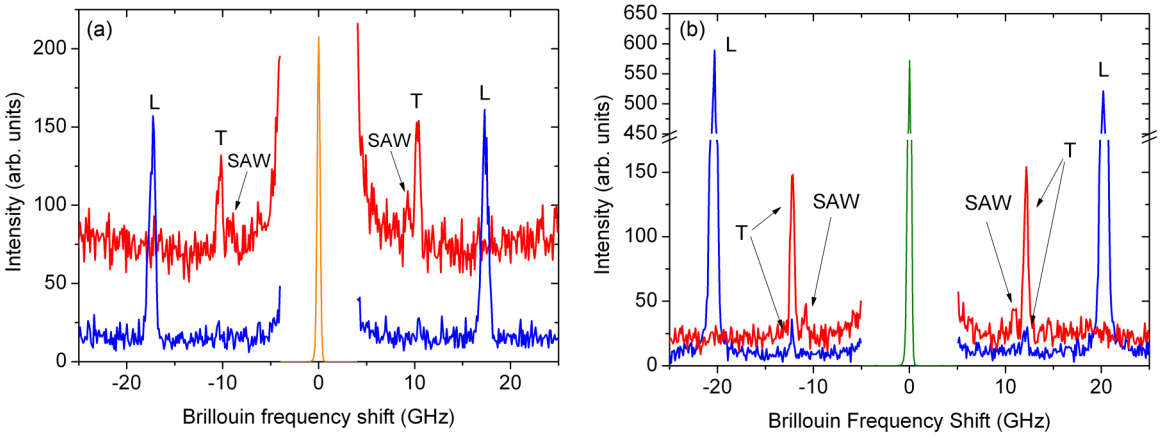

FIG. 4. (a) HRBS spectra of the microscope slab in backscattering geometry for an incident/sagittal angle $\alpha = 50^\circ$ and for *s*-polarized (blue) and *p*- (red) incident light. (b) HRBS spectra of the cover glass in backscattering geometry, inducing the 2αA scattering geometry as explained in the main text ($\alpha = 65^\circ$) for two different polarizations of the incident light, *s* polarized (blue) and *p* polarized (red). *L* and *T* stand for Brillouin peaks related to longitudinal and transverse (shear) acoustic modes.

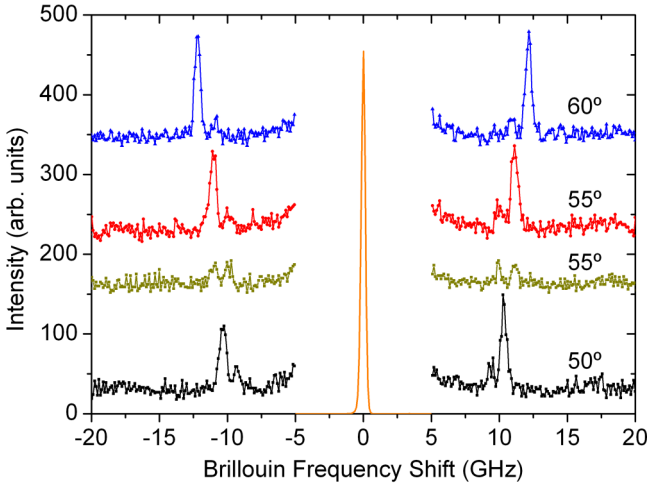

FIG. 5. HRBS spectra of the cover glass in 2αA scattering geometry for different incident/sagittal angles $\alpha = 50^\circ$ (black), $\alpha = 55^\circ$ (red and green), and $\alpha = 60^\circ$ (blue). In the case of $\alpha = 55^\circ$ the red curve is obtained for p-polarized incident light without analysis of the scattered light and the green one is the result with p-analyzed scattered light. The HRBS spectra are vertically shifted for clarity.

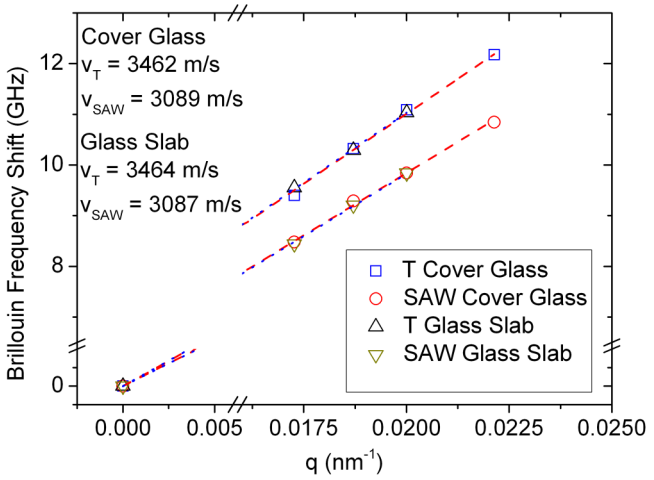

FIG. 6. Dispersion relation of the Brillouin frequency shift with the acoustic wave vector. Open squares and up triangles correspond to cover glass and glass slab bulk shear modes, respectively. Open circles and down triangles correspond to cover glass and glass slab SAW modes, respectively. Red dashed lines and blue dotted lines are the result of nonlinear-squares fits.

This mode of low frequency could be related to the SAW mode of the air-glass interface. In a bulk sample the relevant acoustic SAW mode is the Rayleigh mode and this mode does not change the polarization direction of the scattered light from the polarization of the incident light. This has been tested by placing an analyzer before the spectrometer. The result is clear and can be seen in Fig. 5 where for a sagittal angle $\alpha = 55^\circ$ the depression in the intensity of the peak related to the T mode is clear, while almost no influence in the intensity of the low-frequency mode can be detected.

In both cases, the 2αA scattering geometry and the scattering geometry of the SAW mode, the Brillouin frequency shift is dependent on the scattering angle (or acoustic wave vector) in the same manner. This is clearly shown in Figs. 5 and 6. This low-frequency mode matches all features of a SAW Rayleigh mode.

From the value of the slopes it is straightforward to obtain v_T and v_{SAW}:

$$v_{T,\mathrm{SAW}} = \frac{f^{T,\mathrm{SAW}}\,\lambda_0}{2\,\sin(\alpha)}. \tag{3}$$

The question remains whether this SAW mode arises from the fact of the small thickness of the sample. To answer it, the same experiment as above was performed with a 1-mm-thick microscope slab. In this case the scattering volume is clearly smaller than the thickness of the sample.

As can be seen in Fig. 4(a), the same pattern is reproduced in the case of the microscope slab 1 mm thick. In this case the L and T modes can be seen in either s or p polarization but with much less intensity as in the case of the cover glass. This point is interesting because despite the 1 mm thickness of the sample the reflection of the defocused incident light beam in the back side glass-air interface is still efficient enough to allow the existence of the 2αA scattering geometry. Remember that, as for the previous sample, the incident light beam is focused on the surface of the sample. Much more astonishing is the fact that for the 1-mm-thick microscope slab also a low-frequency mode just below the T mode can be seen. This low-frequency mode behaves like the one observed in the cover glass corresponding to a SAW mode and their frequencies are very similar.

Compared to the calculated values in Table I, the experimental v_{SAW} values are clearly lower (about 3%). This fact is independent of the type of glass studied and seems to be something intrinsic. An error of about 1% could be explained by inaccuracies in the experimental setup, but bigger differences could indicate some slight modification in the physical properties of the surface compared to those of the bulk. Stoddart *et al.* [21] also found differences between the experimental and the calculated SAW velocity values in their study of HRSBS on Si. The existence of a very thin film of native SiO_2 on top of the sample, neglected for the numerical calculations, was for those authors the reason for the found difference. The gathered experimental data for v_{SAW} indicate that the surfaces of these glass plates do not reproduce the expected behavior. It is an open question whether there are some residual stresses or surface absorption of atmospheric molecules (moisture among them) responsible for this inaccuracy.

At this point it has been shown that it is possible to obtain v_{SAW} values from glass transparent samples. Is it also the same in other samples, especially crystalline ones?

In order to answer this question two crystalline platelike samples were investigated. These samples were a 500-μm-thick pristine MgO single-crystalline sample [(001) oriented], a cubic transparent material used typically as a substrate (MaTeck), and a sapphire sample [MaTeck (0001) substrate 500 μm thick]. Sapphire crystals are currently used as substrates for many technological applications, especially in the field of SAW-based devices [22]. This crystal presents crystallographic trigonal (rombohedral) symmetry and from the elastic point of view its basal plane (0001) presents sixfold

TABLE I. Experimental data v_L, v_T, and v_{SAW} and calculated values of the v_{SAW} for microscope slab and cover glass in 90A and b v_{SAW} ackscattering geometry. v_{SAW} values result from the solution of Eq. (1) using the corresponding v_L and v_T as input parameters.

90A scattering geometry	v_L (m/s)	v_T (m/s)	v_{SAW} (m/s) (calculated)	v_{SAW} (m/s) (experimental)
Glass slab	5893 ± 6	3477 ± 35	3187 ± 28	
Cover glass	5858 ± 5	3487 ± 24	3192 ± 20	
Backscattering geometry				
Glass slab	5830 ± 9	3464 ± 10	3171 ± 9	3087 ± 13
Cover glass	5840 ± 5	3462 ± 27	3171 ± 21	3089 ± 20

symmetry for the quasilongitudinal and quasitransverse sound propagation velocities. It is interesting to notice that in both cases in the 90A scattering geometry with the acoustic wave vector lying parallel to the [100] crystallographic direction in the case of MgO and in the case of sapphire parallel to the [100] direction and in a direction 30° from [100], the HRBS spectra show the peaks related to both the T and the L acoustic mode but the peak of the shear acoustic mode is much more intense than that of the L mode (Fig. 7).

This feature is not very common but not unusual, for instance it has also been observed in diamond [23] and recently in Ln : $Ca_3Nb_{1.5}Ga_{3.5}O_{12}$ laser garnets (CNGGs) [24]. It is interesting to notice that these materials present high refractive index values: for MgO $n_{514.5} = 1.7439$ [25], for sapphire in the basal plane $n_{514.5} = 1.7648$ [26], for CNGG $n_{514.5} = 2.2013$ [24], and for diamond $n_{514.5} = 2.4283$ [27].

Typical literature values of MgO sound velocities are shown in Table II. In order to obtain the sound velocity value

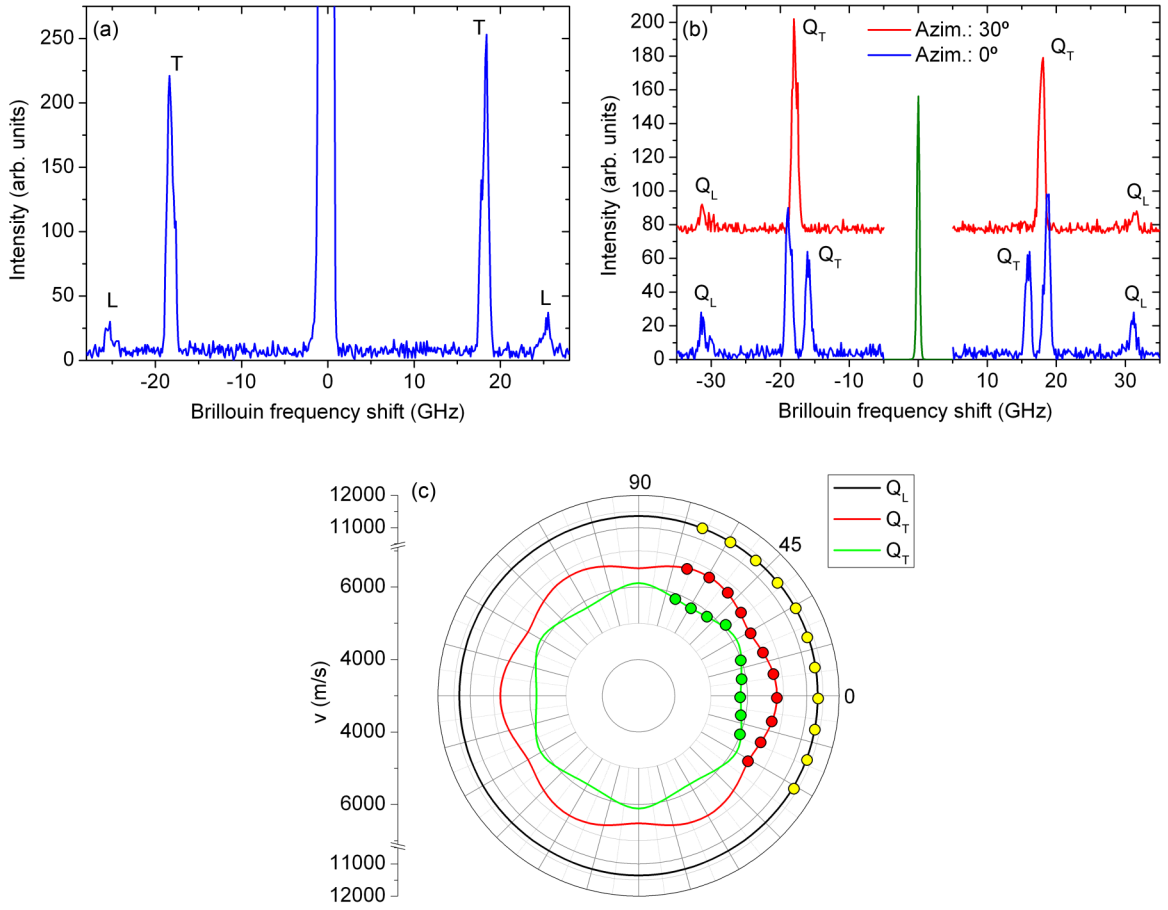

FIG. 7. (a) HRBS spectrum of MgO for the 90A scattering geometry and s-polarized incident light and no analysis of the scattered light. The corresponding acoustic wave vector lies parallel to the [100] crystallographic direction. L and T stand for Brillouin peaks related to longitudinal and transverse (shear) acoustic modes. (b) HRBS spectra of sapphire for the 90A scattering geometry and s-polarized incident light and no analysis of the scattered light. The acoustic wave vector lies parallel to the [100] crystallographic direction in the case of the 0° azimuthal angle. L and T stand for Brillouin peaks related to longitudinal and transverse (shear) acoustic modes. The spectra are vertically shifted for clarity. (c) Polar diagram of the sound velocity curves for sapphire obtained from the HRBS spectra in the (0001) crystallographic plane. The lines are the result of a nonlinear-squares fit of the Christoffel equations. In order to make more visible the sixfold symmetry of the Q_T branches, a zero suppression of 3000 m/s and an axis break in the high values of the y axis were used.

TABLE II. Literature and experimental data for v_L, v_T, v_{SAW} (in the [100] direction), and $(c_{12}/\rho)^{0.5}$, and calculated values of v_{SAW} for MgO in 90A and backscattering geometries. Experimental data for v_L, v_T, v_{SAW} (for an azimuthal angle of 30° from the a axis of the basal plane), and calculated values of v_{SAW} for sapphire in 90A scattering geometry.

Sample	v_L (m/s)	v_T (m/s)	$(c_{12}/\rho)^{0.5}$ (m/s)	v_{SAW} (m/s) (calculated)	v_{SAW} (m/s) (experimental)
MgO (Ref. [28])	9088	6553	5160	5474	–
MgO (90A)	9243 ± 6	6644 ± 6	5366 ± 47	5534	–
MgO (180)	9107 ± 13	6608 ± 17	5407 ± 341	5456	5488 ± 35
Sapphire (90A)	11397 ± 50	6515 ± 5	–	5755	–
Sapphire (180)	–	6488 ± 41	–	–	5715 ± 83

related to the c_{12} elastic constant (independent in the case of cubic symmetry), the sample was rotated an angle 45° about its surface normal (in this way the acoustic wave vector $\vec{q}$ lies parallel to the [110] crystallographic direction) and the Q_L- and Q_T-related Brillouin peaks are easily observed as expected [28]. It is straightforward to calculate $v(c_{12})$ when $v(c_{11})$ and $v(c_{44})$ were already obtained as described above, by solving the Christoffel equation for the [100] and [110] crystallographic directions [27]. The obtained bulk experimental data deliver v_{SAW} calculated values slightly higher than the literature values (Table II). These values were obtained by numerical simulations of Brillouin spectra, originating from surface acoustic excitations, based on the elastodynamic Green's function method that accounts for the surface ripple

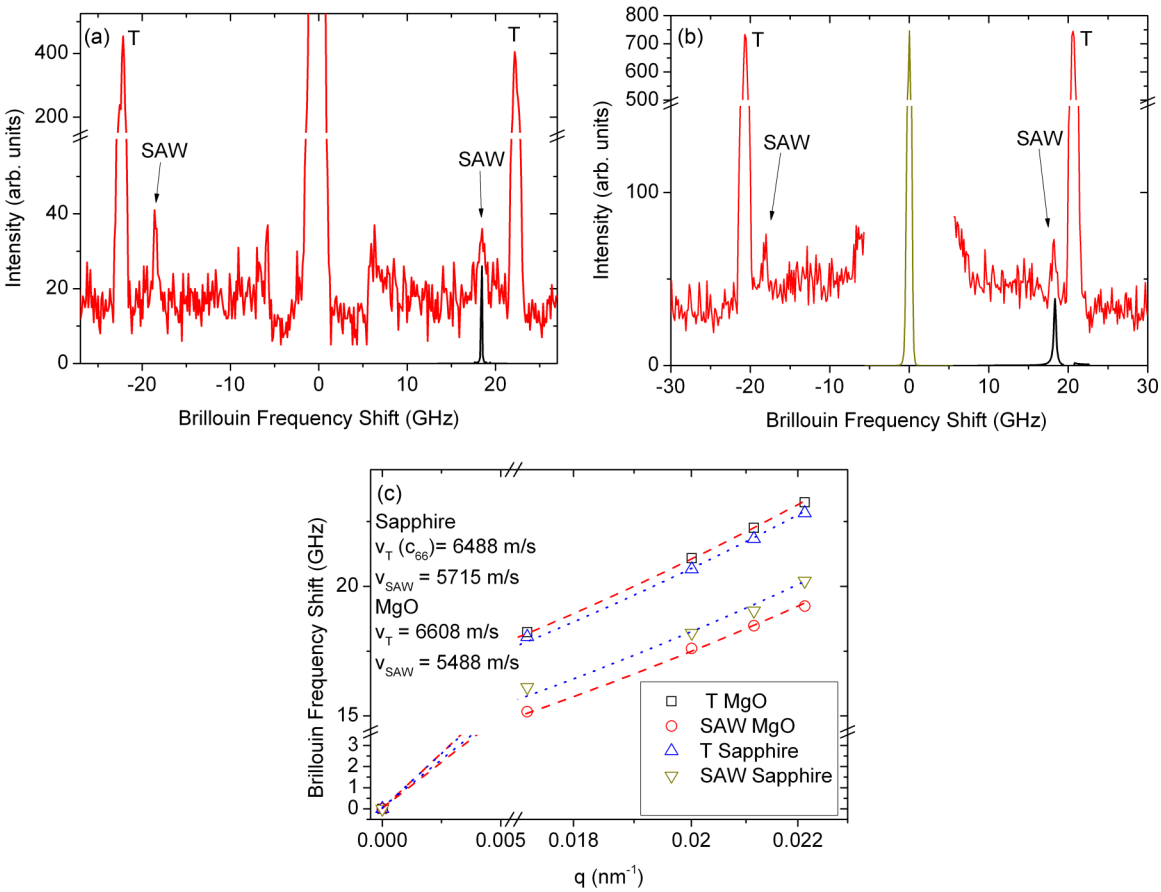

FIG. 8. (a) HRBS spectrum of MgO for the backscattering geometry with an incident/sagittal angle $\alpha = 60°$, p-polarized incident light, and no analysis of the scattered light. The corresponding acoustic wave vector lies parallel to the [100] crystallographic direction. T stands for Brillouin peaks related to transverse (shear) acoustic modes. The Brillouin peak of MgO obtained by numerical simulations of the SAW, propagating parallel to the [100] crystallographic direction, is the black peak. (b) HRBS spectrum of sapphire for the backscattering geometry with an incident/sagittal angle $\alpha = 55°$ and an azimuthal angle of 30°, p-polarized incident light, and no analysis of the scattered light. T stands for Brillouin peaks related to transverse (shear) acoustic modes. The Brillouin peak of sapphire obtained by numerical simulation of the SAW, propagating parallel to the crystallographic direction 30° away from the a axis of the basal plane, is the black peak. (c) Dispersion relation of the Brillouin frequency shift with the acoustic wave vector for MgO and sapphire samples. The straight lines are the result of nonlinear-squares fit. Black squares and blue up triangles correspond to the shear bulk acoustic modes. Red circles and green down triangles correspond to the SAW modes.

mechanism for the inelastic scattering of light [19]. For this numerical simulation the c_{11}, c_{12} and c_{44} values are necessary and the MgO mass density of $\rho = 3583.1\,\mathrm{kg/m^3}$ was assumed [29]. Sapphire presents crystallographic trigonal (rhombohedral) symmetry and from the elastic point of view its basal plane (0001) presents sixfold symmetry for the quasilongitudinal and quasitransverse sound propagation velocities. Typical HRBS spectra for 90A scattering geometry are shown in Fig. 7(b). In this basal plane of a trigonal system only the elastic constants c_{11}, c_{12}, c_{44}, and c_{14} are relevant and they can be determined form the 90A sound velocity experimental data. Thus, from the experimental sound velocity values obtained in 90A scattering geometry and a density of $\rho = 3986\,\mathrm{kg/m^3}$, the expected value of the corresponding v_{SAW} can be obtained in the same way as in the case of MgO [19]. The azimuthal angle of 30° was chosen because the shear mode related to the c_{66} $[(c_{11} - c_{12})/2]$ elastic constant is directly observable [27] and in the case of the sapphire sample is the only shear mode experimentally available [Fig. 7(b)].

In order to couple with the SAW, again sagittal angles around the Brewster angle value (Fig. 1) were selected and the backscattering geometry used. Figures 8(a) and 8(b) show the p polarized backscattering spectrum and the sagittal angle dependence of the bulk shear mode and the SAW Rayleigh mode for both samples.

The experimental values obtained for v_{SAW} directly from the surface Brillouin peaks are also listed in Table II. Within the experimental error the coincidence with the calculated values is very good. It must be pointed out that due to the fact that MgO and sapphire are single crystalline, the inaccuracies in the determination of the direction of the acoustic wave vector $\vec{q}$ when comparing 90A and backscattering geometries are also influenced by the fact that bulk and surface acoustic velocities are also dependent on the crystallographic direction in which $\vec{q}$ is pointing.

IV. CONCLUSIONS

It has been shown that using Brillouin light scattering it is possible to obtain direct information about surface acoustic waves in bulk transparent materials even though the sagittal angle lies around the Brewster angle where almost no reflection of the p-polarized light beam is expected. Despite the fact that the intensities are weak compared to the BLS peaks related to the bulk phonons, there is no intrinsic physical reason for not observing them. The experimental SAW propagation velocities and the results obtained by numerical simulation methods are coincident within the experimental error. However, the quality of the surface plays a very important role in defining the acoustic wave vector properly i.e., the quality of the SBLS peak (the better the surface the easier the detection). This fact reinforces the BLS technique as a nondestructive experimental technique well suited to study both surface and bulk acoustic phonons.

ACKNOWLEDGMENTS

The authors wish to thank Prof. Víctor R. Velasco for encouraging discussions about the character of the detected surface acoustic waves which opened the gates to this research. The research has been possible thanks to the funding from Spanish MINECO under Project No. MAT2012-37276- C03-01, from Comunidad de Madrid Project No. S2013/MIT-2740 (PHAMA_2.0-CM), and from the European Union Seventh Framework Program under Grant Agreement No. 604391 "Graphene Flagship".

[1] D. P. Morgan, Ultrasonics **11**, 121 (1973).
[2] M. J. Vellekoop, Ultrasonics **36**, 7 (1998).
[3] J. R. Sandercock, Solid State Commun. **26**, 547 (1978).
[4] H. Sussner, J. Pelous, M. Schmidt, and R. Vacher, Solid State Commun. **36**, 123 (1980).
[5] B. Mroz and S. Mielcarek, J. Phys. D: Appl. Phys. **34**, 395 (2001).
[6] R. J. Jiménez Riobóo, E. Rodríguez-Cañas, M. Vila, C. Prieto, F. Calle, T. Palacios, M. A. Sánchez, F. Omnès, O. Ambacher, B. Assouar, and O. Elmazria, J. Appl. Phys. **92**, 6868 (2002).
[7] R. J. Jimenez Riobóo and M. Belmahi, J. Appl. Phys. **97**, 073509 (2005).
[8] M. B. Assouar, R. J. Jiménez Riobóo, O. Elmazria, and M. Vila, Diamond Relat. Mater. **16**, 1417 (2007).
[9] G. Carlotti, D. Fioretto, G. Socino, and E. Verona, J. Phys.: Condens. Matter **7**, 9147 (1995).
[10] G. Carlotti, L. Doucet, and M. Dupeux, J. Vac. Sci. Technol. B **14**, 3460 (1996).
[11] E. Salas, F. Jiménez-Villacorta, J. Sánchez-Marcos, R. J. Jiménez Riobóo, A. Muñoz-Martín, J. E. Prieto, V. Joco, and C. Prieto, Phys. Status Solidi A **210**, 513 (2013).
[12] E. Salas, R. J. Jiménez Riobóo, J. Sánchez-Marcos, F. Jiménez-Villacorta, A. Muñoz-Martín, J. E. Prieto, V. Joco, and C. Prieto, J. Appl. Phys. **114**, 213508 (2013).
[13] W. Cheng, R. Sainidou, P. Burgardt, N. Stefanou, A. Kiyanova, M. Efremov, G. Fytas, and P. F. Nealey, Macromolecules **40**, 7283 (2007).
[14] P. Djemia, C. Dugautier, T. Chauveau, E. Dogheche, M. I. Barros, and L. Vandenbulcke, J. Appl. Phys. **90**, 3771 (2001).
[15] J. R. Sandercock, in *Light Scattering in Solids III,* Topics in Applied Physics 51, edited by M. Cardona and G. Güntherodt (Springer, Berlin, 1982), Chap. 6, p. 186.
[16] J. K. Krüger, in *Optical Techniques to Characterize Polymer Systems*, Studies in Polymer Science, Vol. 5, edited by H. Bässler (Elsevier, Amsterdam, 1989), pp. 429–534.
[17] G. W. Farnell, in *Properties of Elastic Surface Waves*, Physical Acoustics, Principles and Methods, Vol. VI, edited by Warren P. Mason (Academic Press, London, 1970), p. 117.
[18] P. C. Vinh and P. G. Malischewsky, Ultrasonics **47**, 49 (2007).
[19] X. Zhang, J. D. Comins, A. G. Every, P. R. Stoddart, W. Pang, and T. E. Derry, Phys. Rev. B **58**, 13677 (1998).
[20] J. K. Krüger, J. Ems, J. Brierley, and R. J. Jiménez Riobóo, J. Phys. D: Appl. Phys. **31**, 1913 (1998).
[21] P. R. Stoddart, J. C. Crowhurst, A. G. Every, and J. D. Commins, J. Opt. Soc. Am. B **15**, 2481 (1998).

[22] O. Ambacher, J. Phys. D: Appl. Phys. **31**, 2653 (1999).
[23] M. H. Grimsditch and A. K. Ramdas, Phys. Lett. A **48**, 37 (1974).
[24] E. Castellano-Hernández, M. D. Serrano, R. J. Jiménez Riobóo, C. Cascales, C. Zaldo, A. Jezowski, and P. A. Loiko, Cryst. Growth Des. **16**, 1480 (2016).
[25] R. E. Stephens and I. H. Malitson, J. Res. Natl. Bur. Stand. **49**, research paper 2360, 249 (1952).
[26] See, for instance, Meller Optics Technical Data for sapphire: http://www.melleroptics.com/data_sheets/Sapphire_Index_of_Refraction.pdf.
[27] F. Peter, Z. Phys. **15**, 358 (1923); H. R. Phillip and E. A. Taft, Phys. Rev. **136**, A1445 (1964).
[28] B. A. Auld, *Acoustic Fields and Waves in Solids*, Vol. 1 (Krieger, Malabar, FL, 1990), p. 395.
[29] K. Marklund and S. A. Mahmoud, Phys. Scr. **3**, 75 (1971).